NATIONAL ADVISORY COMMITTEE FOR AERONAUTICS

TECHNICAL NOTE 2665

AN EXTENSION OF LIFTING ROTOR THEORY TO COVER OPERATION AT LARGE ANGLES OF ATTACK AND HIGH INFLOW CONDITIONS

By Alfred Gessow and Almer D. Crim

Langley Aeronautical Laboratory
Langley Field, Va.

Washington
April 1952

NATIONAL ADVISORY COMMITTEE FOR AERONAUTICS

TECHNICAL NOTE 2665

AN EXTENSION OF LIFTING ROTOR THEORY TO COVER OPERATION AT LARGE ANGLES OF ATTACK AND HIGH INFLOW CONDITIONS

By Alfred Gessow and Almer D. Crim

SUMMARY

Analytical expressions are derived for the flapping, the thrust, the torque, and the profile-drag power of a hinged rotor that are applicable to high-speed helicopters and to certain types of convertible aircraft. The development differs from that used in the standard rotor theory in that no limitation is placed on the magnitude of the blade-section inflow angles and differs also in the treatment of the reversed-velocity region. The equations may be used to calculate the performance of a lifting rotor at any angle of attack either directly or, preferably, from charts.

INTRODUCTION

Present rotor theory (references 1 to 3, for example) has proved to be entirely adequate for predicting the present-day performance of autogiros and helicopters. With the envisioned doubling of the top speed of present-day helicopters, however, and with the advent of convertible aircraft, a review of the assumptions on which the standard rotor theory is based was considered desirable in order to determine the extent to which the theory could be applied to these improved configurations. A review of the theory revealed that the premise that rotor-blade-section inflow angles ϕ are small enough to allow the usual small-angle assumptions that $\cos \phi$ is equal to unity and $\sin \phi$ is equal to ϕ would not apply to the inflow angles generated at the rotors of high-speed, high-performance helicopters or to certain types of convertible aircraft with rotors which operate through a 90° range of angle of attack. Also, for helicopters operating at tip-speed ratios close to 0.5, the high inflow angles (and section angles of attack) usually associated with high-speed flight, together with the relatively large area affected, make the contribution of the reversed-velocity region much more significant than it is at the normally low values of

tip-speed ratio. Consequently, an investigation was made to remove the small-angle and reversed-velocity limitations from the present rotor theory. Just as in the present theory, however, no attempt was made in this investigation to account for blade stall in that part of the rotor disk outside of the reversed-velocity region or for compressibility effects on the blade sections. The results of the investigation are reported herein.

A somewhat similar investigation was made at the Georgia Institute of Technology under the sponsorship and with the financial assistance of the NACA (reference 4). Both of the investigations made use of the idea, first advanced in reference 4, that great simplifications could be effected in the equations for rotor characteristics by representing the angle of attack of a blade section by its sine. (This idea is explained more fully in the section entitled "Basis of Analysis.") The investigations differ, however, in many basic respects, some of major and others of minor significance. The most important differences are as follows: The analysis reported herein is based on the same reference system of axes (that is, the axis of no feathering) as was used in previous NACA works on rotating-wing-aircraft theory (see references 1 and 2); whereas the analysis of reference 4 is based on a system with the axis perpendicular to the rotor tip-path plane. The present analysis also makes use of the "energy" method of calculating rotor losses, a method that readily lends itself to the construction of simplified performance charts, such as those published in reference 3. The analysis of reference 4 uses a "balance of force" method for calculating rotor losses that entails the calculation of the longitudinal component of force in the tip-path plane (that is, the so-called "H" force). The two investigations also differ significantly in the manner in which the reversed-velocity region is handled. It is expected that the analysis presented in this paper will be most applicable to aircraft having rotors with flapping blades, whereas an analysis based on tip-path-plane axes might be applied more conveniently to rigid-rotor aircraft.

SYMBOLS

Physical Quantities

b	number of blades per rotor
R	blade radius measured from center of rotation, feet
r	radial distance to blade element, feet
x	ratio of blade-element radius to rotor-blade radius (r/R)

c blade-section chord, feet

c_e equivalent blade chord (on thrust basis), feet $\left(\frac{\int_0^R cr^2 dr}{\int_0^R r^2 dr}\right)$

σ rotor solidity $(bc_e/\pi R)$

θ blade-section pitch angle; angle between line of zero lift of blade section and plane perpendicular to axis of no feathering, radians

θ_0 blade pitch angle at hub, radians

θ_1 difference between hub and tip pitch angles; positive when tip angle is larger, radians

I_1 mass moment of inertia of a blade about flapping hinge, slugs per square foot

γ mass constant of rotor blade; expresses ratio of air forces to mass forces $\left(c\rho aR^4/I_1\right)$

ρ mass density of air, slugs per cubic foot

Air-Flow Parameters

V true airspeed of helicopter along flight path, feet per second

Ω rotor angular velocity, radians per second

α rotor angle of attack; angle between axis of no feathering (that is, axis about which there is no cyclic-pitch change) and plane perpendicular to flight path, positive when axis is pointing rearward, degrees

v induced inflow velocity at rotor (always positive), feet per second

μ tip-speed ratio $\left(\frac{V \cos \alpha}{\Omega R}\right)$

λ inflow ratio $\left(\frac{V \sin \alpha - v}{\Omega R}\right)$

ψ blade azimuth angle measured from downwind position in direction of rotation, radians

U_T component at blade element of resultant velocity perpendicular to blade-span axis and to axis of no feathering, feet per second

u_T nondimensional component of resultant velocity at blade element $(U_T/\Omega R)$

U_P component at blade element of resultant velocity perpendicular both to blade-span axis and U_T, feet per second

u_P nondimensional component of resultant velocity at blade element $(U_P/\Omega R)$

U resultant velocity perpendicular to blade-span axis at blade element, feet per second

u nondimensional resultant velocity at blade element $(U/\Omega R)$

ϕ inflow angle at blade element in plane perpendicular to blade-span axis, radians $\left(\tan^{-1} \frac{U_P}{U_T}\right)$

α_r blade-element angle of attack, measured from line of zero lift, radians $(\theta + \phi)$

Aerodynamic Characteristics

c_l section lift coefficient

$\bar{c}_l$ average section lift coefficient in reversed-velocity region

c_{d_o} section profile-drag coefficient

$\bar{c}_{d_o}$ average section profile-drag coefficient in reversed-velocity region

$\delta_0, \delta_1, \delta_2$ coefficients in power series expressing c_{d_o} as a function of α_r $\left(c_{d_o} = \delta_0 + \delta_1 \alpha_r + \delta_2 \alpha_r^2\right)$

a slope of curve of section lift coefficient against section angle of attack (radian measure)

C_1, C_2, C_3, C_4 and $K_1, K_2, K_3, \ldots$ coefficients for use in profile-drag torque and power expressions

L lift, pounds

T rotor thrust, pounds

Q rotor-shaft torque, pound-feet

P_o rotor-shaft profile-drag power, pound-feet per second

C_T thrust coefficient $\left(\frac{T}{\pi R^2 \rho (\Omega R)^2}\right)$

C_Q rotor-shaft torque coefficient $\left(\frac{Q}{\pi R^2 \rho (\Omega R)^2 R}\right)$

C_{P_o} rotor-shaft profile-drag power coefficient $\left(\frac{P_o}{\pi R^2 \rho (\Omega R)^3}\right)$

B tip-loss factor; blade elements outboard of radius BR are assumed to have profile drag but no lift

Rotor-Blade Motion

β blade flapping angle at particular azimuth position measured from plane perpendicular to axis of no feathering, radians

a_0 constant term in Fourier series that expresses β (radians); hence, the rotor coning angle

a_n coefficient of $\cos n\psi$ in Fourier series that expresses β

b_n coefficient of $\sin n\psi$ in Fourier series that expresses β

Subscripts:

i	induced
o	profile
f	"forward-velocity" region
r	reversed-velocity region (except in α_r)
l	component due to lift vector
d	component due to drag vector
.75R	at 0.75 radius
std	standard theory
ext	extended theory

BASIS OF ANALYSIS

Although the general development of the thrust, torque, and blade-flapping equations that is given in the following section is similar to that for the standard theory presented in references 1 and 2, the omission of the small-angle assumptions in the equations of this paper and the consideration of higher tip-speed ratios result in differences between the development of the two sets of equations. These departures from conventional rotor theory are now discussed.

(1) The elemental thrust at a blade section used in deriving the thrust and thrust-moment equations is taken as the projection of the elemental lift vector on the axis of no feathering instead of being assumed equal to the elemental lift. The component of the profile-drag vector in the thrust direction is also considered in calculating the thrust and thrust moment in the reversed-velocity region. (As a result of many sample computations, it was concluded that the profile-drag component is negligible everywhere except in the reversed-velocity region.) Similarly, exact components of the elemental lift and drag vectors are used in deriving the torque equations. (See fig. 1.)

(2) The resultant velocity U is used instead of U_T in computing the lift and drag at each element. (See fig. 1.) Radial (that is, spanwise) components of velocities are ignored as usual, although such

velocity components may significantly affect the blade drag at extremely high tip-speed ratios.

(3) When flight up to tip-speed ratios of 0.5 is considered, the contributions of the reversed-velocity region become a significantly large part of the total thrust, torque, and power produced by the rotor, inasmuch as high inflow angles (and section angles of attack) are usually present at the high tip-speed ratios that produce the relatively large reversed-velocity areas. (This statement is principally true for the helicopter power-on flight condition. For other flight conditions, such as partial-power helicopter descents or autorotative operation at high tip-speed ratios, large reversed-velocity areas may exist with small inflow angles.) The contribution of the reversed-velocity region to the rotor characteristics is computed in the rotor theory of references 1 and 2 by assuming that the blade sections in that region, as well as those in the forward-velocity part of the disk, remain unstalled no matter how high the angles of attack encountered in that region may be. Because the standard rotor theory is also based on the assumption that the resultant velocity at a blade section can be represented by the tangential component of velocity U_T, the assumption of no stall in the reversed-velocity region does not normally seriously overestimate the thrust and accelerating torque, inasmuch as the overestimation of the lift coefficient is somewhat compensated for by the underestimation of the dynamic pressure at each blade section. The underestimation of the decelerating torque and the profile-drag power is much more significant, however, because the effects of the two assumptions are additive in those cases. When the normal component of velocity U_P is included in the resultant velocity at each section, as is done in this paper, and when large areas of reversed velocity and high section angles of attack are present, the effect of the no-stall assumption results in further errors because the thrust and accelerating torque contributions are greatly overestimated, and the decelerating torque and profile-drag power contributions to the total thrust, torque, and power are underestimated.

These effects were investigated for a sample practical operating condition $\left(\mu = 0.4,\ C_T = 0.00362,\ \theta_0 = 24^\circ,\ \theta_1 = -12^\circ\right)$ by numerical step-by-step calculations. The results showed that the thrust produced by the reversed-velocity region, calculated on the basis of unstalled flow and with U_P considered in the section resultant velocity, is about 23 percent of that produced by the rest of the disk, whereas the contribution is only 8 percent when calculated on the basis of stalled flow. For the same sample case, the profile-drag power contribution of the reversed-velocity region is 18 percent of that produced by the rest of the disk when calculated by means of the no-stall assumption, whereas this contribution is 51 percent when calculated with stall considered. In addition to illustrating the errors that could be introduced by not considering the effects of stall in the reversed-velocity region at high

speeds, these data point up the fact that the contributions of the reversed-velocity region can be quite significant.

In order to account for the stalled flow in the reversed-velocity region in a relatively simple manner, advantage is taken of the fact that the average section angle of attack in this region for most tip-speed ratios and power-on flight conditions is extremely and uniformly high. (For these conditions, a typical value of section angle of attack is 60°.) The section lift and drag coefficients in this region are therefore assumed to be constant. The trust, torque, and power equations are then developed by first calculating the contributions of the "forward-velocity" region (that is, the area outside the reversed-velocity region) and then algebraically adding to them the contributions of the reversed-velocity region computed on the basis of constant lift and drag coefficients.

Calculation of rotor characteristics in the reversed-velocity region requires certain further assumptions of a semiempirical nature even though such assumptions are not necessary for the forward-velocity region. The approximations used in the reversed-velocity region are pointed out as they arise in the development of the analysis and are subsequently shown to be satisfactory over a wide range of operating conditions.

(4) Preliminary investigations of the problem of computing rotor characteristics without making the usual small-angle assumptions for θ and ϕ showed that the resulting equations for rotor thrust, torque, and blade flapping motion are too unwieldy for analytic solution. In order to make the equations amenable to practical solution, advantage is taken of the fact that, although the pitch angle or the section inflow angle separately may be too large for the small-angle assumptions to apply, their sum may not be if the rotor is to operate with the significant elements not highly stalled. It is therefore permissible to use α_r and $\sin \alpha_r$ interchangeably. (Even at $\alpha_r = 20°$, the error due to this assumption is only about 2 percent.) In practice the substitution of $\sin \alpha_r$ for α_r in the expressions for the lift and drag coefficient of a blade element makes it possible to develop the equations for rotor forces without the previously adopted restrictions of θ and ϕ to small angles.

The analysis given in the following section is developed, as are those given in references 1 and 2, for linearly twisted, rectangular blades with the flapping hinge located on the rotor center and perpendicular to the rotor axis and to the blade span. All velocities, forces, and moments are referred to the axis of no feathering. An explanation of this system of axes, together with means for applying the equations based on this system to pure feathering or combination flapping-feathering systems, is given in reference 5.

ANALYSIS

Thrust.- From reference 1, the velocity components at a rotor blade element may be expressed nondimensionally as

$$u_T = \frac{U_T}{\Omega R} = x + \mu \sin \psi \tag{1}$$

$$u_P = \frac{U_P}{\Omega R} = \lambda + \frac{1}{2}\mu a_1 + \left(-\mu a_0 + x b_1 + \frac{1}{2}\mu a_2\right)\cos \psi + \left(-x a_1 + \frac{1}{2}\mu b_2\right)\sin \psi +$$

$$\left(\frac{1}{2}\mu a_1 + 2x b_2\right)\cos 2\psi + \left(\frac{1}{2}\mu b_1 - 2x a_2\right)\sin 2\psi \tag{2}$$

and

$$u = \frac{U}{\Omega R} = \left(u_T^2 + u_P^2\right)^{1/2} \tag{3}$$

Also, from figure 1,

$$\left.\begin{aligned} U_T &= U \cos \phi \\ \text{or} \qquad u_T &= u \cos \phi \end{aligned}\right\} \tag{4}$$

$$\left.\begin{aligned} U_P &= U \sin \phi \\ \text{or} \qquad u_P &= u \sin \phi \end{aligned}\right\} \tag{5}$$

Again, from figure 1, the rotor thrust at a blade element with the drag component neglected is found to be

$$dT = dL \cos \phi \tag{6}$$

where, from simple blade-element theory,

$$dL = c_l \frac{1}{2}\rho U^2 c \, dr \tag{7}$$

On the assumption that

$$\alpha_r = \sin \alpha_r \tag{8}$$

and that the lift-curve slope is constant, c_l may be expressed as

$$c_l = a \sin \alpha_r = a \sin\left(\theta_0 + x\theta_1 + \phi\right) \tag{9}$$

If equation (9) is expanded by the standard trigonometric identities, and the result combined with equations (4) to (7), then

$$\frac{dT}{dr} = \frac{1}{2}\rho ac\left[\left(\sin \theta_0 \cos x\theta_1 + \cos \theta_0 \sin x\theta_1\right)U_T^2 + \left(\cos \theta_0 \cos x\theta_1 - \sin \theta_0 \sin x\theta_1\right)U_T U_P\right] \tag{10}$$

The total thrust produced over the "forward-velocity" region (that is, that part of the rotor disk over which the flow is not reversed) by a rotor of b blades is

$$T_f = \frac{b}{2\pi}\int_0^{2\pi}\int_0^{BR} \frac{dT}{dr} \, dr \, d\psi - \frac{b}{2\pi}\int_\pi^{2\pi}\int_0^{-\mu R \sin \psi} \frac{dT}{dr} \, dr \, d\psi \tag{11}$$

Before equation (10) is substituted into equation (11) and the indicated integrations are performed, it was found desirable first to expand $\cos x\theta_1$ and $\sin x\theta_1$ by the following terms of the power series:

$$\left.\begin{aligned}\cos x\theta_1 &= 1 - \frac{(x\theta_1)^2}{2!} + \frac{(x\theta_1)^4}{4!} \\ \sin x\theta_1 &= (x\theta_1) - \frac{(x\theta_1)^3}{3!} + \frac{(x\theta_1)^5}{5!}\end{aligned}\right\} \tag{12}$$

The series expansion was used in the integration instead of exactly integrating the terms containing $\cos x\theta_1$ and $\sin x\theta_1$ in order to avoid a discontinuous result in the integrated answer at $\theta_1 = 0$ and to avoid the necessity of having to use a very large number of significant figures in obtaining a numberical value of the thrust for small values of θ_1.

Substituting equations (1), (2), (10), and (12) into equation (11) and integrating on the basis that the chord c is constant gives an expression for the thrust produced by the forward-velocity region. The expression can be made nondimensional by substituting into it the expressions for C_T and σ that are listed in the section entitled "Symbols." When these substitutions are made, the final expression becomes, after simplification,

$$\left(\frac{2C_T}{\sigma a}\right)_f = \sin\theta_0\left[\frac{B^3}{3} + \mu^2\frac{B}{2} - \frac{2}{9\pi}\mu^3 - \theta_1\left(\lambda\frac{B^3}{3} + \frac{1}{9\pi}\mu^3\lambda\right) - \theta_1^2\left(\frac{B^5}{10} + \mu^2\frac{B^3}{12}\right) + \theta_1^3\lambda\frac{B^5}{30} + \theta_1^4\frac{B^7}{168}\right] + \cos\theta_0\left[\lambda\frac{B^2}{2} + \mu^2 b_2\frac{B}{4} + \mu^2\frac{\lambda}{8} + \mu^3\frac{a_1}{16} + \theta_1\left(\frac{B^4}{4} + \mu^2\frac{B^2}{4} - \frac{\mu^4}{64}\right) + \theta_1^2\left(\frac{\mu^4\lambda}{128} - \lambda\frac{B^4}{8}\right) - \theta_1^3\left(\frac{B^6}{36} + \mu^2\frac{B^4}{48}\right)\right] \tag{13}$$

The simplifications expressed in equation (13) were made by neglecting all terms in μ of higher order than the fourth and by omitting all terms that contributed but negligibly to the final result; the latter terms being determined from numerical examples representing extreme flight conditions. These same simplifications were also made in the final expression for the flapping, rotor torque, and rotor profile-drag power coefficients which are subsequently developed.

The thrust produced by the lift vectors in the reversed-velocity region T_{r_l} is calculated on the basis that the lift coefficient remains

constant, so that

$$T_{r_l} = b \frac{1}{2}\rho c \bar{c}_l \frac{1}{2\pi} \int_{\pi}^{2\pi} d\psi \int_{0}^{-\mu R \sin\psi} U^2 \cos \phi \, dr \tag{14}$$

Inasmuch as exact evaluation of the last integral in equation (14) is not feasible, an approximation of the $U^2 \cos \phi$ term by an expression that is readily integrated is necessary. The semiempirical relationships employed are as follows:

$$U^2 \cos \phi = U_T U \cong U_T \left(U_P - \frac{U_T}{2} \right)$$

$$\cong U_T \left[|\lambda| \left(1 - \frac{\mu}{2} \right) \Omega R + \frac{U_T}{2} \right] \tag{15}$$

In the preceeding equation, U_P is replaced by the expression

$$U_P = u_P \Omega R \cong \lambda \left(1 - \frac{\mu}{2} \right) \Omega R \tag{16}$$

which is based on the assumption that U_P varies linearly from a value of λ at the blade root to zero at the blade tip. The same expression for U_P is also used in deriving the reversed-velocity contributions to the rotor torque and power. The bracketed expression in equation (15) is made a positive quantity by placing absolute bars about λ, inasmuch as the expression replaces the resultant velocity U, which is always positive.

Evaluating equation (14) with the aid of equation (15) and making the answer nondimensional gives the expression for the reversed-velocity thrust as

$$\left(\frac{2C_T}{\sigma a} \right)_{r_l} = \frac{\bar{c}_l}{a} \left[\frac{1}{8} \mu^2 |\lambda| \left(1 - \frac{\mu}{2} \right) + \frac{\mu^3}{9\pi} \right] \tag{17}$$

It should be noted that $\bar{c}_l$ is positive when λ is positive, and negative when λ is negative, inasmuch as the reversed-velocity

thrust acts upward in normal power-off flight and downward in power-on flight.

As mentioned in the previous section, the contribution of the profile drag to the total thrust is negligible in the forward-velocity region. In the region of reversed flow, however, the profile-drag contribution T_{r_d} becomes significant because of large inflow angles and high profile-drag values resulting from the stalled flow and is given by the following expression:

$$T_{r_d} = b\,\frac{1}{2}\rho c\bar{c}_{d_o}\,\frac{1}{2\pi}\int_{\pi}^{2\pi} d\psi \int_{0}^{-\mu R\sin\psi} U^2 \sin\phi\, dr \tag{18}$$

The use of the same assumptions employed for equation (15) yields

$$U^2\sin\phi = U_P U \cong \lambda\Omega R\left(1 - \frac{\mu}{2}\right)\left(U_P - \frac{U_T}{2}\right)$$

$$\cong \lambda\Omega R\left(1 - \frac{\mu}{2}\right)\left[|\lambda|\left(1 - \frac{\mu}{2}\right)\Omega R + \frac{U_T}{2}\right] \tag{19}$$

Substituting equation (19) into (18), integrating, and making the result nondimensional gives the following expression

$$\left(\frac{2C_T}{\sigma a}\right)_{r_d} = \frac{\bar{c}_{d_o}}{a}\left[\frac{\mu}{\pi}\lambda|\lambda|\left(1 - \frac{\mu}{2}\right) + \frac{\mu^2\lambda}{16}\right]\left(1 - \frac{\mu}{2}\right) \tag{20}$$

The total rotor thrust coefficient can then be obtained as the sum of equations (13), (17), and (20); thus,

$$\frac{2C_T}{\sigma a} = \left(\frac{2C_T}{\sigma a}\right)_f + \left(\frac{2C_T}{\sigma a}\right)_{r_l} + \left(\frac{2C_T}{\sigma a}\right)_{r_d} \tag{21}$$

Blade motion.- The motion of a flapping blade can be described by a Fourier series that expresses the relation between the flapping angle β and the blade azimuth angle ψ. To a degree of accuracy sufficient for most purposes, the series can be written as

$$\beta = a_0 - a_1 \cos \psi - b_1 \sin \psi - a_2 \cos 2\psi - b_2 \sin 2\psi \qquad (22)$$

Equations for determining the five unknown coefficients in equation (22) are obtained by equating the sum of the blade thrust, centrifugal force, and inertia moments about the blade-flapping hinge to zero.

The thrust moment at any value of ψ may be written as

$$M_T = \int_0^{BR} \frac{1}{2}\rho c U^2 c_l r \, dr = \int_0^{BR} \frac{dT}{dr} r \, dr - \left[\int_0^{-\mu R \sin\psi} \frac{dT}{dr} r \, dr \right]_{\pi}^{2\pi} +$$

$$\left[\int_0^{-\mu R \sin\psi} \frac{1}{2}\rho c \left[\bar{c}_l U^2 \cos \phi + \bar{c}_{d_o} U^2 \sin \phi \right] r \, dr \right]_{\pi}^{2\pi} . \qquad (23)$$

where the notation $\Big]_{\pi}^{2\pi}$ is used to indicate that the expression enters into the thrust moment only in the interval between $\psi = \pi$ and $\psi = 2\pi$. The elemental thrust moment dTr can be obtained by simply multiplying equation (10) by r. The last integral in equation (23), which represents the moments contributed by the lift and profile-drag components in the reversed-velocity region, can be evaluated by means of equations (15) and (19). (As in equation (17), the sign of $\bar{c}_l$ is dependent upon the sign of λ.)

Evaluating equation (23) and following the method used in reference 1 results in the following five simultaneous equations for use in determining the five flapping coefficients:

$$a_0 = \frac{\gamma}{2}\Bigg\{ \cos\theta_0 \left[\frac{B^3}{3}\lambda + \frac{1}{8}\mu^2 b_2 B^2 + 0.0398\lambda\mu^3 + 0.033 a_1 \mu^4 + \theta_1\left(\frac{B^5}{5} + \frac{1}{6}\mu^2 B^3\right) - \frac{\theta_1^2}{2}\left(\frac{B^5}{5}\lambda\right) - \frac{\theta_1^3}{6}\left(\frac{B^7}{7}\right)\right] +$$

$$\sin\theta_0 \left[\frac{B^4}{4} + \frac{B^2}{4}\mu^2 - \frac{1}{64}\mu^4 - \theta_1\left(\lambda\frac{B^4}{4} + \frac{1}{64}\lambda\mu^4\right) - \frac{\theta_1^2}{4}\left(\frac{B^6}{3} + \frac{B^4}{4}\mu^2\right) + \frac{\theta_1^3}{12}\left(\frac{B^6}{3}\lambda\right) + \frac{\theta_1^4}{96}\left(\frac{B^8}{2}\right)\right] +$$

$$\frac{1}{128a}\mu^4 \bar{c}_l + \frac{1}{8a}|\lambda|\lambda\mu^2\left(1 - \frac{\mu}{2}\right)^2 \bar{c}_{d_o} + \frac{0.0398}{a}\mu^3|\lambda|\left(1 - \frac{\mu}{2}\right)\bar{c}_l + \frac{0.0199}{a}\lambda\left(1 - \frac{\mu}{2}\right)\mu^3 \bar{c}_{d_o}\Bigg\} \qquad (24)$$

$$0 = \cos\theta_0\left[-\mu\frac{B^3}{3}a_0 + \frac{1}{4}b_1B^4 + \frac{\mu^2b_1B^2}{8} - 0.050a_2\mu^4 - \frac{\mu B^3a_2}{6} - \frac{\theta_1^2}{2}\left(-\mu\frac{B^5}{5}a_0 + \frac{b_1B^6}{6}\right)\right] - \sin\theta_0\left[\theta_1\left(-\frac{\mu B^4}{4}a_0 + b_1\frac{B^5}{5} + \mu^2b_1\frac{B^3}{12} - \frac{\mu B^4a_2}{8}\right) + \theta_1^3\left(-\frac{b_1B^7}{42}\right)\right] \tag{25}$$

$$0 = \sin\theta_0\left[\frac{2}{3}\mu B^3 + 0.0265\mu^4 - \theta_1\left(\mu\lambda\frac{B^3}{3} - a_1\frac{B^5}{5} + \frac{\mu^2}{12}a_1B^3 - \frac{\mu}{8}b_2B^4 - 0.0265\lambda\mu^4\right) - \frac{\theta_1^2}{2}\left(\frac{2}{5}\mu B^5\right) - \theta_1^3\left(\frac{a_1B^7}{42} - \frac{\mu^2a_1B^5}{120}\right)\right] + \cos\theta_0\left[\mu\frac{\lambda}{2}B^2 - a_1\frac{B^4}{4} + \frac{\mu^2a_1B^2}{8} - \frac{\mu B^3b_2}{6} - \frac{1}{32}a_1\mu^4 - \frac{1}{16}\lambda\mu^3 + \theta_1\left(\mu\frac{B^4}{2}\right) - \frac{\theta_1^2}{2}\left(\mu\lambda\frac{B^4}{4} - \frac{a_1B^6}{6} + \mu^2a_1\frac{B^4}{16}\right) - \frac{\theta_1^3}{6}\left(\frac{\mu B^6}{3}\right) + \frac{\theta_1^4}{24}\left(-\frac{a_1B^8}{8}\right)\right] - 0.01325\mu^4\frac{\bar{c}_l}{a} - 0.2123\lambda|\lambda|\mu^2\left(1 - \frac{\mu}{2}\right)^2\frac{\bar{c}_{d_o}}{a} - \frac{1}{16}\mu^3|\lambda|\left(1 - \frac{\mu}{2}\right)\frac{\bar{c}_l}{a} - \frac{1}{32}\lambda\left(1 - \frac{\mu}{2}\right)\mu^3\frac{\bar{c}_{d_o}}{a} \tag{26}$$

$$a_2 = \frac{\gamma}{6}\left\{\sin\theta_0\left[-\frac{1}{4}\mu^2B^2 + \frac{1}{64}\mu^4 - \theta_1\left(\mu a_1\frac{B^4}{4} + 2b_2\frac{B^5}{5}\right) + \frac{\theta_1^2}{2}\left(\frac{1}{8}\mu^2B^4\right)\right] + \right.$$

$$\cos\theta_0\left[\frac{\mu B^3}{3}a_1 + \frac{B^4b_2}{2} + 0.0265\lambda\mu^3 + 0.0150a_1\mu^4 + \theta_1\left(-\frac{\mu^2}{6}B^3\right) - \right.$$

$$\left.\left.\frac{\theta_1^2}{2}\left(\mu\frac{B^5}{5}a_1 + \frac{B^6}{3}b_2\right)\right] - \frac{1}{128a}\mu^4\bar{c}_l - \frac{1}{8a}\lambda|\lambda|\mu^2\left(1 - \frac{\mu}{2}\right)^2\bar{c}_{d_o} + \right.$$

$$\left.\frac{0.0265}{a}\mu^3|\lambda|\left(1 - \frac{\mu}{2}\right)\bar{c}_l + \frac{0.01327}{a}\lambda\left(1 - \frac{\mu}{2}\right)\mu^3\bar{c}_{d_o}\right\} \tag{27}$$

$$b_2 = \frac{\gamma}{6}\left\{\cos\theta_0\left[-\mu^2a_0\frac{B^2}{4} + \frac{\mu B^3}{3}b_1 - a_2\frac{B^4}{2} + \frac{1}{16}a_2\mu^4 + \right.\right.$$

$$\left.\left.\frac{\theta_1^2}{2}\left(\frac{\mu B^5}{5}b_1 - a_2\frac{B^6}{3}\right)\right] - \sin\theta_0\left[\theta_1\left(-\mu^2a_0\frac{B^3}{6} + \mu b_1\frac{B^4}{4} - \frac{2}{5}a_2B^5\right)\right]\right\} \tag{28}$$

Accelerating torque.- As was done in reference 2, the torque arising from the inclination of the lift vectors relative to the plane perpendicular to the axis of no feathering is called the "accelerating" torque in the present paper, even though such torque tends to accelerate the rotor only in the case of power-off operation.

The differential expression for the accelerating torque (see fig. 1) may be written as

$$\frac{dQ_i}{dr} = \frac{1}{2}\rho U^2c_l\sin\phi\ cr\ dr \tag{29}$$

which, after substitution from equations (4), (5), and (9), becomes

$$\frac{dQ_i}{dr} = \frac{1}{2}\rho ac\left[\sin\left(\theta_0 + \theta_1 x\right)U_P U_T + \cos\left(\theta_0 + \theta_1 x\right)U_P{}^2\right]r \tag{30}$$

The accelerating torque produced by the forward velocity region is then

$$Q_{i_f} = \frac{b}{2\pi}\int_0^{2\pi} d\psi \int_0^{BR} \frac{dQ_i}{dr}\,dr - \frac{b}{2\pi}\int_\pi^{2\pi} d\psi \int_0^{-\mu R\sin\psi} \frac{dQ_i}{dr}\,dr \tag{31}$$

Evaluating equation (31) with the aid of equations (1), (2), (12), and (30), and nondimensionalizing and simplifying the result gives the following expression

$$\left(\frac{2C_{Q_i}}{\sigma a}\right)_f = \sin\theta_0\left[\frac{\lambda}{3}B^3 + \frac{1}{8}\mu^2 b_2 B^2 - \frac{\theta_1{}^2}{2}\left(\frac{\lambda B^5}{5}\right) + \frac{1}{9\pi}\mu^3\lambda + C_1\left(-\frac{\theta_1 B^3}{3} + \frac{\theta_1{}^3 B^5}{30}\right) + C_2\left(-\frac{\theta_1}{4}B^4\right) + C_3\left(-\frac{\theta_1 B^5}{5}\right)\right] + \cos\theta_0\left[\theta_1\left(\frac{\lambda}{4}B^4 + \frac{1}{12}\mu^2 b_2 B^3\right) - \frac{\theta_1{}^3}{6}\left(\frac{\lambda}{6}B^6\right) + C_1\left(\frac{B^2}{2} - \theta_1{}^2\frac{B^4}{8}\right) + C_2\left(\frac{B^3}{3}\right) + C_3\left(\frac{B^4}{4} - \theta_1{}^2\frac{B^6}{12}\right) - \frac{1}{2}\left(\frac{1}{4}\mu^2\lambda^2 + \frac{3}{8}\mu^3 a_1\lambda\right)\right] \tag{32}$$

where

$$C_1 = \lambda^2 + \mu a_1\lambda + \frac{1}{2}\mu^2 a_0{}^2 + \frac{3}{8}\mu^2 a_1{}^2 + \frac{1}{8}\mu^2 b_1{}^2 - \frac{1}{2}\mu^2 a_0 a_2 \tag{33}$$

$$C_2 = -\mu a_0 b_1 + \frac{1}{2}\mu a_1 b_2 - \frac{1}{2}\mu b_1 a_2 \tag{34}$$

$$C_3 = \frac{1}{2} a_1^2 + \frac{1}{2} b_1^2 + 2a_2^2 + 2b_2^2 \tag{35}$$

The accelerating torque produced by the reversed-velocity region is

$$Q_{i_r} = \frac{b}{2\pi} \int_{\pi}^{2\pi} d\psi \int_{0}^{-\mu R \sin\psi} \frac{1}{2} \rho c U^2 \sin \phi \bar{c}_l r \, dr \tag{36}$$

The approximation is made that $U^2 \sin \phi \cong U_P^2$. Using the value of U_P as given by equation (16), substituting into equation (36), integrating and nondimensionalizing the answer yields the following expression for the accelerating torque in the reversed-velocity region

$$\left(\frac{2C_{Q_i}}{\sigma a}\right)_r = - \frac{\bar{c}_l}{8a} \mu^2 \lambda |\lambda| \left(1 - \frac{\mu}{2}\right)^2 \tag{37}$$

The total accelerating torque is then the sum of equations (32) and (37)

$$\frac{2C_{Q_i}}{\sigma a} = \left(\frac{2C_{Q_i}}{\sigma a}\right)_f + \left(\frac{2C_{Q_i}}{\sigma a}\right)_r \tag{38}$$

Decelerating torque.- The decelerating or profile-drag torque produced by b blade elements (see fig. 1) is

$$dQ_o = bc_{d_o} \frac{1}{2} \rho c U^2 \cos \phi \, r \, dr \tag{39}$$

where, as in reference 2, c_{d_o} is expressed as

$$c_{d_o} = \delta_0 + \delta_1 \alpha_r + \delta_2 \alpha_r^2 \tag{40}$$

When equation (39) is expanded with the aid of equations (4), (5), (9), and (40), the following expression is obtained:

$$dQ_o = \frac{1}{2}\rho bc \left\{ \delta_0 \frac{U_T^2}{\cos \phi} + \delta_1 \left[\sin(\theta_0 + \theta_1 x) U_T^2 + \cos(\theta_0 + \theta_1 x) U_P U_T \right] + \right.$$

$$\delta_2 \left[\sin^2(\theta_0 + \theta_1 x) U_T^2 + \cos^2(\theta_0 + \theta_1 x) U_P^2 + \right.$$

$$\left. \left. U_P U_T \sin 2(\theta_0 + \theta_1 x) \right] \cos \phi \right\} r \, dr \qquad (41)$$

Although the assumption that $\alpha_r = \sin \alpha_r$ was successful in eliminating terms involving $\sin \phi$ and $\cos \phi$ from the integral equations for thrust, thrust moment, and accelerating torque, $\cos \phi$ terms still remain in equation (41). As will be shown in the succeeding section entitled "Discussion," a subsequent investigation showed that $\cos \phi$ could be assumed equal to unity in equation (41) with small error in the final answer for Q_o in most cases, even in the most extreme operating conditions when ϕ is very large. The validity of such an assumption is aided by the fact that, in the normal operating angle-of-attack range, the δ_0 and δ_2 terms are of the same order of magnitude. Since $\cos \phi$ appears in the denominator of the δ_0 term and in the numerator of the δ_2 term, the effects of $\cos \phi$ tend to cancel each other.

The decelerating torque contributed by the forward velocity region, as represented by the nondimensional coefficient, is

$$\left(\frac{2C_{Q_o}}{\sigma} \right)_f = \frac{1}{2\pi} \int_0^{2\pi} d\psi \int_0^{1.0} \frac{dC_{Q_o}}{dx} dx - \frac{b}{2\pi} \int_\pi^{2\pi} d\psi \int_0^{-\mu \sin \psi} \frac{dC_{Q_o}}{dx} dx \qquad (42)$$

Substituting equations (1), (2), (12), and the nondimensional form of equation (41) into equation (42) and integrating results in the following expression for $\left(\frac{2C_{Q_o}}{\sigma} \right)_f$:

$$\left(\frac{2C_{Q_o}}{\sigma}\right)_f = K_1\left(\frac{1}{4} + \frac{1}{4}\mu^2\right) + K_2\left(\frac{1}{5} + \frac{1}{6}\mu^2\right) + K_3\left(\frac{1}{6} + \frac{1}{8}\mu^2\right) + K_4\left(\frac{1}{7} + \frac{1}{10}\mu^2\right) +$$

$$K_5\left(\frac{1}{8} + \frac{1}{12}\mu^2\right) + K_6\left(\frac{1}{9} + \frac{1}{14}\mu^2\right) + K_7\left(\frac{1}{3}\lambda + \frac{1}{8}\mu^2 b_2\right) +$$

$$K_8\left(\frac{1}{4}\lambda + \frac{1}{12}\mu^2 b_2\right) + K_9\left(\frac{1}{5}\lambda + \frac{1}{16}\mu^2 b_2\right) + K_{10}\left(\frac{1}{6}\lambda + \frac{1}{20}\mu^2 b_2\right) +$$

$$K_{11}\left(\frac{1}{7}\lambda + \frac{1}{24}\mu^2 b_2\right) + K_{12}\left(\frac{1}{8}\lambda + \frac{\mu^2 b_2}{28}\right) + C_1\left(\frac{1}{2}K_{13} + \frac{1}{3}K_{14} +\right.$$

$$\left.\frac{1}{4}K_{15} + \frac{1}{5}K_{16} + \frac{1}{6}K_{17} + \frac{1}{7}K_{18}\right) + C_2\left(\frac{1}{3}K_{13} + \frac{1}{4}K_{14} + \frac{1}{5}K_{15} +\right.$$

$$\left.\frac{1}{6}K_{16} + \frac{1}{7}K_{17} + \frac{1}{8}K_{18}\right) + C_3\left(\frac{1}{4}K_{13} + \frac{1}{5}K_{14} + \frac{1}{6}K_{15} + \frac{1}{7}K_{16} +\right.$$

$$\left.\frac{1}{8}K_{17} + \frac{1}{9}K_{18}\right) - C_4\frac{K_{13}}{2} - K_1\frac{\mu^4}{64} + K_7\frac{1}{9\pi}\mu^3\lambda + K_8\frac{1}{64}\mu^4\lambda \qquad (43)$$

where C_1, C_2, and C_3 are as defined in formulas (33) to (35) and

$$C_4 = \frac{1}{4}\mu^2\lambda^2 + \frac{3}{8}\mu^3 a_1\lambda + \frac{1}{16}\mu^4 a_0^2 \qquad (44)$$

$$K_1 = \delta_0 + \delta_1 \sin\theta_0 + \delta_2 \sin^2\theta_0 \qquad (45)$$

$$K_7 = \delta_1 \cos\theta_0 + \delta_2 \sin 2\theta_0 \qquad (46)$$

$$K_8 = \left(-\delta_1 \sin\theta_0 + 2\delta_2 \cos 2\theta_0\right)\theta_1 \qquad (47)$$

$$K_9 = \left(-\frac{1}{2}\delta_1 \cos\theta_0 - 2\delta_2 \sin 2\theta_0\right)\theta_1^2 \tag{48}$$

$$K_{10} = \left(\frac{1}{6}\delta_1 \sin\theta_0 - \frac{4}{3}\delta_2 \cos 2\theta_0\right)\theta_1^3 \tag{49}$$

$$K_{11} = \left(\frac{1}{24}\delta_1 \cos\theta_0 + \frac{2}{3}\delta_2 \sin 2\theta_0\right)\theta_1^4 \tag{50}$$

$$K_2 = K_7\theta_1 \tag{51}$$

$$K_3 = \frac{1}{2}K_8\theta_1 \tag{52}$$

$$K_4 = \frac{1}{3}K_9\theta_1 \tag{53}$$

$$K_5 = \frac{1}{4}K_{10}\theta_1 \tag{54}$$

$$K_6 = \frac{1}{5}K_{11}\theta_1 \tag{55}$$

$$K_{12} = \left(-\frac{1}{120}\delta_1 \sin\theta_0 + \frac{4}{15}\delta_2 \cos 2\theta_0\right)\theta_1^5 \tag{56}$$

$$K_{13} = \delta_2 \cos^2\theta_0 \tag{57}$$

$$K_{14} = -\delta_2 \sin 2\theta_0\theta_1 \tag{58}$$

$$K_{15} = -\delta_2 \cos 2\theta_0\theta_1^2 \tag{59}$$

$$K_{16} = \frac{2}{3}\delta_2 \sin 2\theta_0\theta_1^3 \tag{60}$$

$$K_{17} = \frac{1}{3}\delta_2 \cos 2\theta_0\theta_1^4 \tag{61}$$

$$K_{18} = -\frac{2}{15}\delta_2 \sin 2\theta_0\theta_1^5 \tag{62}$$

It should be noted that the K constants defined by the preceding equations are functions only of the pitch angle, blade twist, and the section drag characteristics.

The decelerating torque coefficient for the reversed-velocity region is

$$(Q_o)_r = \frac{1}{2\pi}\int_{\pi}^{2\pi} d\psi \int_0^{-\mu R\sin\psi} \frac{1}{2}\rho bc\bar{c}_{d_o} U^2 \cos\phi \; r \; dr \tag{63}$$

If the value of $U^2\cos\phi$ as given by equation (15) is substituted into equation (63), made nondimensional, and then integrated, the result is

$$\left(\frac{2C_{Q_o}}{\sigma}\right)_r = -\bar{c}_{d_o}\left[\frac{\mu^3}{9\pi}|\lambda|\left(1 - \frac{\mu}{2}\right) + \frac{\mu^4}{128}\right] \tag{64}$$

The resultant decelerating torque contribution is obtained as the sum of equations (43) and (64):

$$\frac{2C_{Q_o}}{\sigma} = \left(\frac{2}{\sigma}C_{Q_o}\right)_f + \left(\frac{2}{\sigma}C_{Q_o}\right)_r \tag{65}$$

Profile-drag power.- The differential expression for the profile-drag power can be written as

$$dP_o = b\,\frac{1}{2}\rho c c_{d_o} U^3 dr \tag{66}$$

Expanding equation (66) with the aid of equations (3), (4), (5), (9), and (40), and expressing the results in nondimensional form, gives

$$dC_{P_o} = \frac{\sigma}{2}\left\{\delta_0\left(u_T^2 + u_P^2\right)\frac{u_T}{\cos\phi} + \delta_1\left[\frac{u_T^2}{\cos^2\phi}\,U_P\cos\left(\theta_0 + \theta_1 x\right) + \left(u_T^3 + u_P^2 u_T\right)\sin\left(\theta_0 + \theta_1 x\right)\right] + \delta_2\left[\frac{u_T}{\cos\phi}\,u_P^2\cos^2\left(\theta_0 + \theta_1 x\right) + \frac{u_T^3}{\cos\phi}\sin^2\left(\theta_0 + \theta_1 x\right) + \frac{u_T^2}{\cos\phi}\,u_P\sin 2\left(\theta_0 + \theta_1 x\right)\right]\right\} \qquad (67)$$

As in equation (41), it was found that the omission of the $\cos\phi$ terms in equation (67) results in an error of but a few percent in the final answer.

The total profile-drag power contributed by the foward-velocity region can be written as

$$\left(\frac{2}{\sigma}C_{P_o}\right)_f = \frac{1}{2\pi}\int_0^{2\pi} d\psi \int_0^1 \frac{dC_{P_o}}{dx}\,dx - \frac{1}{2\pi}\int_\pi^{2\pi} d\psi \int_0^{-\mu\sin\psi} \frac{dC_{P_o}}{dx}\,dx \qquad (68)$$

After substitution, integration, and simplification, the final expression for $\left(\frac{2}{\sigma}C_{P_o}\right)_f$ becomes:

$$\left(\frac{2}{\sigma} C_{P_o}\right)_f = K_1\left(\frac{1}{4} + \frac{3}{4}\mu^2\right) + K_2\left(\frac{1}{5} + \frac{1}{2}\mu^2\right) + K_3\left(\frac{1}{6} + \frac{3}{8}\mu^2\right) + K_4\left(\frac{1}{7} + \frac{3}{10}\mu^2\right) +$$

$$K_5\left(\frac{1}{8} + \frac{1}{4}\mu^2\right) + K_6\left(\frac{1}{9} + \frac{3}{14}\mu^2\right) + \frac{3}{64}K_1\mu^4 + \left(\lambda - \frac{1}{2}\mu a_1\right)\left(\frac{1}{3}K_7 +$$

$$\frac{1}{4}K_8 + \frac{1}{5}K_9 + \frac{1}{6}K_{10} + \frac{1}{7}K_{11} + \frac{1}{8}K_{12}\right) + \left(\frac{1}{2}\mu^2\lambda + \frac{1}{8}\mu^3 a_1\right)\left(K_7 +$$

$$\frac{1}{2}K_8 + \frac{1}{3}K_9 + \frac{1}{4}K_{10} + \frac{1}{5}K_{11} + \frac{1}{6}K_{12}\right) - \frac{2}{9\pi}\mu^3\lambda K_7 - \frac{1}{64}\mu^4\lambda K_8 +$$

$$\left(\frac{1}{2}\mu^2 b_2\lambda - \frac{1}{4}\mu^3 a_0 b_1\right)\left(K_{19} + \frac{1}{2}K_{20} + \frac{1}{3}K_{21} + \frac{1}{4}K_{22} + \frac{1}{5}K_{23} +\right.$$

$$\left.\frac{1}{6}K_{24}\right) + \left(\lambda^2 + \frac{1}{2}\mu^2 a_0^2 + \frac{1}{8}\mu^2 a_1^2 + \frac{3}{8}\mu^2 b_1^2 + \frac{1}{2}\mu^2 a_0 a_2\right)\left(\frac{1}{2}K_{19} +\right.$$

$$\left.\frac{1}{3}K_{20} + \frac{1}{4}K_{21} + \frac{1}{5}K_{22} + \frac{1}{6}K_{23} + \frac{1}{7}K_{24}\right) + \left(-\mu a_0 b_1 + \frac{3}{2}\mu a_1 b_2 -\right.$$

$$\left.\frac{3}{2}\mu b_1 a_2\right)\left(\frac{1}{3}K_{19} + \frac{1}{4}K_{20} + \frac{1}{5}K_{21} + \frac{1}{6}K_{22} + \frac{1}{7}K_{23} + \frac{1}{8}K_{24}\right) +$$

$$\left(\frac{1}{2}a_1^2 + \frac{1}{2}b_1^2 + 2a_2^2 + 2b_2^2\right)\left(\frac{1}{4}K_{19} + \frac{1}{5}K_{20} + \frac{1}{6}K_{21} + \frac{1}{7}K_{22} +\right.$$

$$\left.\frac{1}{8}K_{23} + \frac{1}{9}K_{24}\right) + \left(\frac{1}{2}K_{19}\right)\left(\frac{1}{4}\mu^2\lambda^2 + \frac{1}{4}\mu^3 a_1\lambda + \frac{1}{16}\mu^4 a_0^2\right) +$$

$$K_{20}\left(\frac{1}{9\pi}\mu^3\lambda^2\right) \qquad (69)$$

where K_1 to K_{18} are expressed by equations (45) to (62) and

$$K_{19} = \delta_0 + \delta_1 \sin\theta_0 + \delta_2 \cos^2\theta_0 \tag{70}$$

$$K_{20} = \left(\delta_1 \cos\theta_0 - \delta_2 \sin 2\theta_0\right)\theta_1 \tag{71}$$

$$K_{21} = \left(-\frac{1}{2}\delta_1 \sin\theta_0 - \delta_2 \cos 2\theta_0\right)\theta_1^2 \tag{72}$$

$$K_{22} = \left(-\frac{1}{6}\delta_1 \cos\theta_0 + \frac{2}{3}\delta_2 \sin 2\theta_0\right)\theta_1^3 \tag{73}$$

$$K_{23} = \left(\frac{1}{24}\delta_1 \sin\theta_0 + \frac{1}{3}\delta_2 \cos 2\theta_0\right)\theta_1^4 \tag{74}$$

$$K_{24} = \left(\frac{1}{120}\delta_1 \cos\theta_0 - \frac{2}{15}\delta_2 \sin 2\theta_0\right)\theta_1^5 \tag{75}$$

The profile-drag power for the reversed-velocity region is

$$\left(P_o\right)_r = \frac{1}{2\pi}\int_{\pi}^{2\pi} d\psi \int_0^{-\mu R \sin\psi} \frac{1}{2}\rho b c \bar{c}_{d_o} U^3 dr \tag{76}$$

The variable part of the integral in equation (76) can be handled as follows:

$$U^3 = \left(U_T^2 + U_P^2\right)U \cong \left(U_T^2 + U_P^2\right)\left[U_T - \frac{1}{2}|\lambda|\Omega R\left(1 - \frac{\mu}{2}\right)\right] \tag{77}$$

Substituting the value for U_P obtained from equation (16) into equation (77), substituting the result into equation (76), integrating, and nondimensionalizing permits the power loss in the reversed-velocity region to be expressed by

$$\left(\frac{2c_{P_o}}{\sigma}\right)_r = \bar{c}_{d_o}\left[\frac{3}{64}\mu^4 + |\lambda|\left(1 - \frac{\mu}{2}\right)\frac{\mu^3}{9\pi} + \frac{1}{8}\mu^2\lambda^2\left(1 - \frac{\mu}{2}\right)^2 + \frac{\mu}{2\pi}\lambda^2|\lambda|\left(1 - \frac{\mu}{2}\right)^3\right] \tag{78}$$

The total profile-drag power coefficient is then determined as the sum of equations (69) and (78):

$$\frac{2}{\sigma} C_{P_o} = \left(\frac{2}{\sigma} C_{P_o}\right)_f + \left(\frac{2}{\sigma} C_{P_o}\right)_r \tag{79}$$

DISCUSSION

Check of simplifications and assumptions.- A number of assumptions and simplifications (among which are the assumption that section lift and drag coefficients in the reversed-velocity region could be represented by uniform stalled values, the simplifications used in the reversed-velocity region, and the neglect of some $\cos \phi$ terms in the profile-drag torque and power equations) have been made in deriving the rotor equations.

In order to determine the effect of these approximations on the accuracy of the theory derived in this paper, rotor characteristics for a number of different flight conditions were calculated by the theoretical equations, and the answers have been compared with those obtained by a step-by-step integration performed on automatic computing machines. The step-by-step method eliminated all small-angle assumptions and the assumption that the resultant velocity at the blade element U (without the radial component of flow) could be replaced by the tangential component U_T. The method also permitted section stall in the reversed-velocity region to be considered, although stall was not considered by either method in the forward-velocity region. The same lift and drag curves were used by both methods in the forward-velocity region and were represented by

$$\left.\begin{aligned} c_l &= 5.73\alpha_r \\ c_{d_o} &= 0.0087 - 0.0216\alpha_r + 0.400\alpha_r^2 \end{aligned}\right\} \tag{80}$$

In the reversed-velocity region, the analytical method assumed that

$$\left.\begin{aligned} \bar{c}_l &= 1.2 \\ \bar{c}_{d_o} &= 1.1 \end{aligned}\right\} \tag{81}$$

whereas the step-by-step method utilized the lift and drag curves shown in figure 2. The curves in figure 2 are arbitrary and were devised to simulate, in an approximate manner, the characteristics of an airfoil section up to high angles of attack.

The ratios of values of thrust, accelerating torque, decelerating torque, and power obtained by the two methods are plotted against the inflow angle ϕ at the tip of the advancing blade (fig. 3). The values of rotor angle of attack, tip-speed and inflow ratios, and blade pitch and twist angles corresponding to each of the flight conditions are also indicated in the figure. It can be seen that good agreement exists between the extended theory and step-by-step methods of computing rotor characteristics throughout the range of inflow angles investigated. (The highest values of inflow angles covered correspond to operation at tip-speed ratios of 0.5 or to operation at large rotor angles of attack such as might occur at steep climb angles. The theory is expected to be applicable for any value of ϕ encountered in helicopter or convertible-aircraft flight.) It may therefore be concluded that the assumptions and approximations used in deriving the present theory are justified by the simplifications of the relationships they permit and by the good agreement of the results of the theory with those obtained by an exact step-by-step analysis.

Comparison between standard and extended theories.- Essentially, the difference between the standard and extended theories lies in the fact that the extended theory omits the small-angle assumptions in the forward- and reversed-velocity regions and takes stall and the profile-drag contribution to the thrust into account in the reversed-velocity area. For relatively low-speed and cruising level flight, or at moderate rates of climb and descent, the two theories should give substantially the same results, whereas in high-speed flight or at large angles of climb or descent different results would be expected. It is of interest to determine the range of flight conditions at which the two theories begin to diverge, and also the maximum extent to which the differences in small-angle and reversed-velocity assumptions affect the rotor equations.

A comparison of the thrust equation as herein developed with that given by the standard theory in reference 1 reveals that, aside from differences in the reversed-velocity terms, the removal of the small-angle assumption resulted in the replacing of θ by $\sin\theta$ in the equation and in modifying all other terms by $\cos\theta$. For a constant forward speed (or constant μ) condition, therefore, the blade pitch angle θ lends itself for use as a convenient parameter by which the two theories can be compared.

In order to illustrate the comparison with a sample case, calculations by both theories of thrust, accelerating and decelerating torques,

and profile-drag power of a sample rotor having blades with -8° twist are plotted in figure 4. The results, which are presented in each figure in the form of ratios of values as computed by the two theories, are plotted against the three-quarter-radius pitch angle. (The accelerating torque curves of figure 4 are plotted in the form of absolute values, rather than ratios, because in the region of low or zero torque the ratios would become meaningless.) The maximum values of $\theta_{.75R}$ shown on the plots would be about the maximum values that might be expected in normal helicopter operation. Very much larger angles might possibly be employed in the rotors of certain types of convertible aircraft with rotors which are also used as propellers. In such cases, low values of μ may be combined with very high values of θ. Curves are shown for three values of tip-speed ratio (0.1, 0.3, and 0.5) and for two values of $2C_T/\sigma a$ (0.03 and 0.01). The higher value of $2C_T/\sigma a$ represents an upper limit from the standpoint of rotor stall at the higher tip-speed ratios, whereas the lower value represents the value near which most high-speed helicopters will tend to operate.

A study of the plots of figure 4 indicates that the two theories give essentially the same answers (within 10 percent) at low values of μ over the range of $\theta_{.75R}$ values shown. If curves for the low values of μ were extrapolated to higher $\theta_{.75R}$ values, significant differences could be seen to occur at those pitch values at which the rotors of certain types of convertible aircraft might be expected to operate. At high values of μ, the two theories differ by very large amounts, the differences varying markedly with θ. Thus the extended theory would seem to be more applicable than the standard theory for calculating the performance of rotors operating in the power-on condition at very large angles of attack or at tip-speed ratios exceeding approximately 0.25.

It might be pointed out that the thrust equation (equation (13)) is particularly sensitive to the effects of θ in that small errors arising from the replacement of $\sin\theta$ by θ and $\cos\theta$ by 1 are magnified in the equation because the $\sin\theta$ and $\cos\theta$ terms are of approximately equal magnitudes. For the power-on case, the two sets of terms are subtracted from one another, and the answer, being a small difference between two large numbers, can be very much in error.

Selection of average lift and drag coefficients in reversed-velocity region.- As previously pointed out, it is possible, in autorotation for example, for large reversed-velocity regions to exist in which the mean angle of attack is quite small as compared with the high, usually stalled, values in the power-on condition. The proper choice of the average lift and drag coefficient values to be used in calculating the reversed-velocity region would therefore depend on the flight condition.

For most power-on flight conditions, the numerical calculations discussed in this section indicate the following values to be satisfactory: $\bar{c}_l = 1.2$; $\bar{c}_{d_o} = 1.1$. For the autorotative flight condition, values of $\bar{c}_l$ and $\bar{c}_{d_o}$ in the neighborhood of 0.5 and 0.1, respectively, seem to be reasonable. For other flight conditions, other values of $\bar{c}_l$ and $\bar{c}_{d_o}$ might be more appropriate.

LIMITATIONS OF THEORY

As stated in the preceding section, the extended theory of this paper is expected to be applicable for any range of inflow angles encountered in helicopter or convertible-aircraft flight. Also pointed out was the fact that the semiempirical approximations used in handling the reversed-velocity region were satisfactory over the wide range of flight conditions that were investigated numerically, which included tip-speed ratios up to 0.5. Although the numerical check of the theory tends to inspire confidence in its application to somewhat greater values of μ, the use of the reversed-velocity region approximations, as exemplified by equations (15), (16), and (77), and the omission of the radial velocity component, probably will result in a loss in accuracy of the theory at the higher tip-speed ratios, particularly in the calculation of the rotor profile-drag torque and profile-drag power. It is difficult, in fact, to evaluate accurately by analytical means the degree of error in estimating the rotor drag brought about by ignoring the radial-velocity components of the resultant velocities at each of the blade elements at any tip-speed ratio.

The possible reduction in accuracy at tip-speed ratios much beyond 0.5 does not place a significant limitation on the theory, inasmuch as rotors operating at the very high values of μ will necessarily be lightly loaded, at which condition the relative importance of the profile-drag terms becomes less as compared with the other power absorbing items, such as parasite and possibly auxiliary-wing drag. If a relatively high degree of accuracy is desired at the higher values, the errors introduced into the theory by the approximations and omissions should be analytically or experimentally investigated.

Inasmuch as blade stall was considered specifically only in the reversed-velocity region, the extended theory, just as standard rotor theory, is limited to conditions of operation wherein excessive stall does not exist outside the reversed-velocity boundary. The effects of moderate amounts of stall on profile-drag power may be estimated by the method suggested in reference 6. Blade stall limitations, which have

been shown to occur simultaneously with conditions of optimum performance in reference 6, may be estimated by the methods given in references 2 and 3 for the standard rotor theory.

Limited experimental tests and calculations indicate that compressibility effects on rotors operating at high tip speeds may substantially alter the aerodynamic characteristics of the rotor, the primary effect being an increase in profile-drag power. The theory of this paper does not account for these losses because of the added complexity involved and the lack of suitable airfoil data at high Mach numbers and high angles of attack. When such section data, as well as more extensive experimental rotor data, do become available, it is expected that compressibility power losses may be accounted for in a manner similar to that used for stall effects.

Since some high-speed helicopters and convertible aircraft will probably be operating at relatively high disk loading and torque values, an investigation of the effect on the equations of the approximation of tip losses by a constant tip-loss factor B and of the ommission of a rotational-inflow factor was considered advisable. Therefore a comparison was made of the results of the extended theory, modified for the vertical-flight condition, with those of the Goldstein propeller theory, for a few different vertical-flight conditions. The cases investigated included conditions of relatively high inflow, torque, and disk loading, as might be encountered by rotors used in certain types of convertible aircraft, as well as more conventional helicopter loadings. The comparison indicated that, at least for the vertical-flight condition, the use of the widely used constant tip-loss factor $B = 0.97$ yielded answers for rotor characteristics that are in close agreement with those given by the more exact Goldstein propeller theory. A similar check for the forward flight condition could not be made because of the lack of a rigorous method of calculating tip losses in that condition. The question becomes much less important in high-speed flight, however, inasmuch as induced losses are comparatively low at high speeds.

APPLICATION OF THEORY

The equations of blade flapping, thrust, torque, and profile-drag power were developed in terms of the three fundamental variables; namely, λ, θ, and μ. Different combinations of these variables may be inserted into the equations in order to obtain the characteristics of rotors in different flight conditions. Inasmuch as the equations are lengthy when applied to twisted blades, if a large number of different rotors or flight conditions are to be investigated, the equations can be used to prepare charts (similar to those given in reference 3) from which the rotor characteristics can be obtained directly.

Although the equations of this paper were developed for rectangular blades, experience (obtained with the theory of reference 2, which was

also developed for constant-chord blades) has shown that such equations may be applied successfully to blades of conventional tapered plan form by the use of an equivalent chord c_e for calculating the solidity ratio.

CONCLUDING REMARKS

An extension of rotor theory has been presented to obtain analytical expressions for rotor flapping coefficients, thrust, torque, and profile-drag power that are not limited by the small-angle assumptions for blade pitch and inflow angles used in standard rotor theory. In addition, because the contribution of the reversed-velocity region becomes significantly large in high-speed rotor flight, it was necessary in the derivation to account for blade stall in this region. The equations are therefore expected to be applicable to high-speed helicopters and to certain types of convertible aircraft. Just as in standard rotor theory, the equations are limited to conditions of moderate amounts of stall on the blade sections outside of the reversed-velocity region and do not include Mach number effects.

A comparison of the equations of the extended theory with those of the standard rotor theory indicates that the extended theory should be used in predicting the characteristics of rotors operating in the power-on condition at very high angles of attack or at tip-speed ratios exceeding approximately 0.25.

Langley Aeronautical Laboratory
National Advisory Committee for Aeronautics
Langley Field, Va., December 4, 1951

REFERENCES

1. Wheatley, John B.: An Aerodynamic Analysis of the Autogiro Rotor with a Comparison between Calculated and Experimental Results. NACA Rep. 487, 1934.

2. Bailey, F. J., Jr.: A Simplified Theoretical Method of Determining the Characteristics of a Lifting Rotor in Forward Flight. NACA Rep. 716, 1941.

3. Bailey, F. J., Jr., and Gustafson, F. B.: Charts for Estimation of the Characteristics of a Helicopter Rotor in Forward Flight. I - Profile Drag-Lift Ratio for Untwisted Rectangular Blades. NACA ACR L4H07, 1944.

4. Castles, Walter, Jr., and New, Noah C.: A Blade Element Analysis for Lifting Rotors That Is Applicable for Large Inflow and Blade Angles and Any Reasonable Blade Geometry. NACA TN 2656, 1952.

5. Gessow, Alfred: Standard Symbols for Helicopters. NACA TN 1604, 1948.

6. Gustafson, F. B., and Gessow, Alfred: Effect of Blade Stalling on the Effeciency of a Helicopter Rotor as Measured in Flight. NACA TN 1250, 1947.

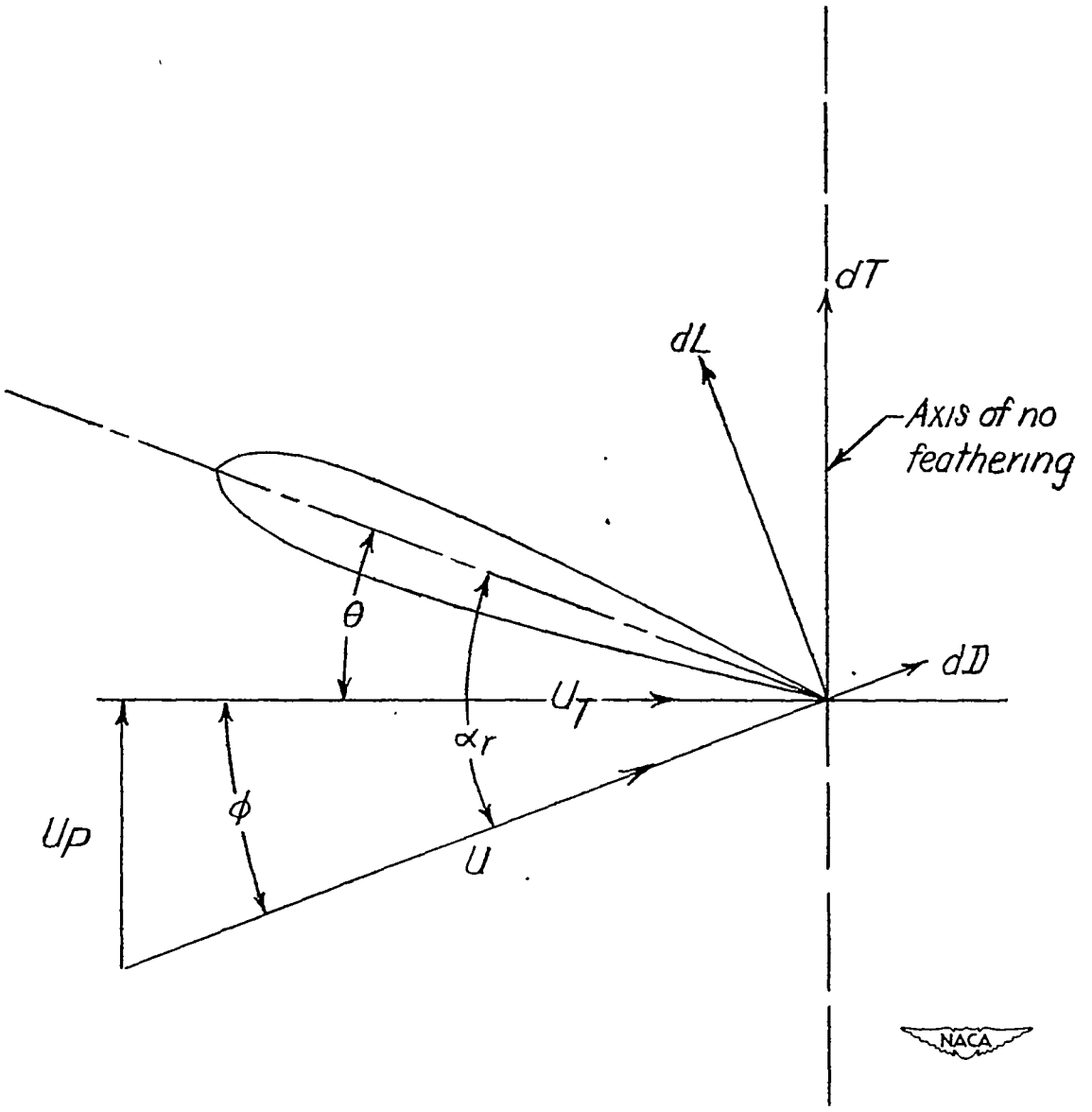

Figure 1.- Diagram of velocities and flow angles at blade element.

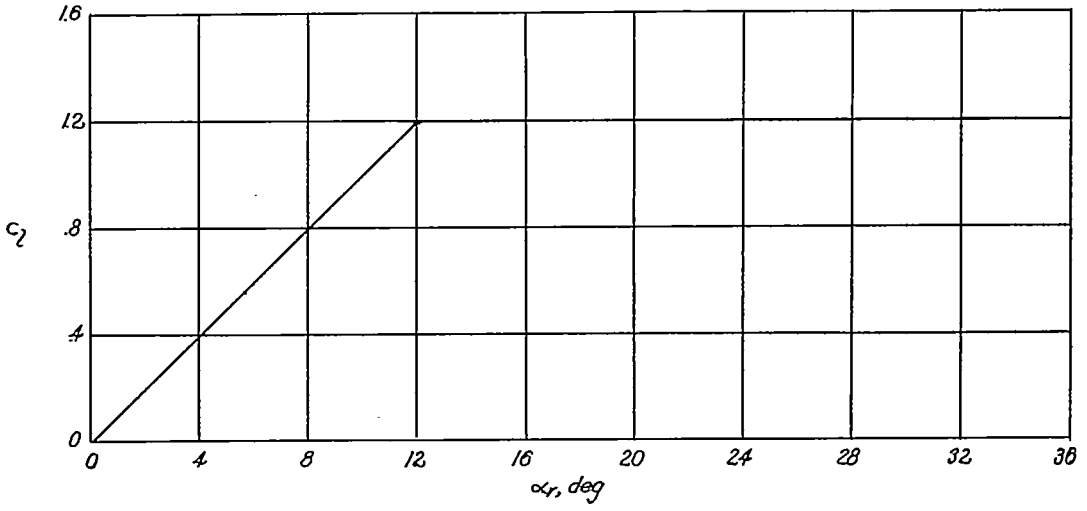

(a) c_l plotted against α_r.

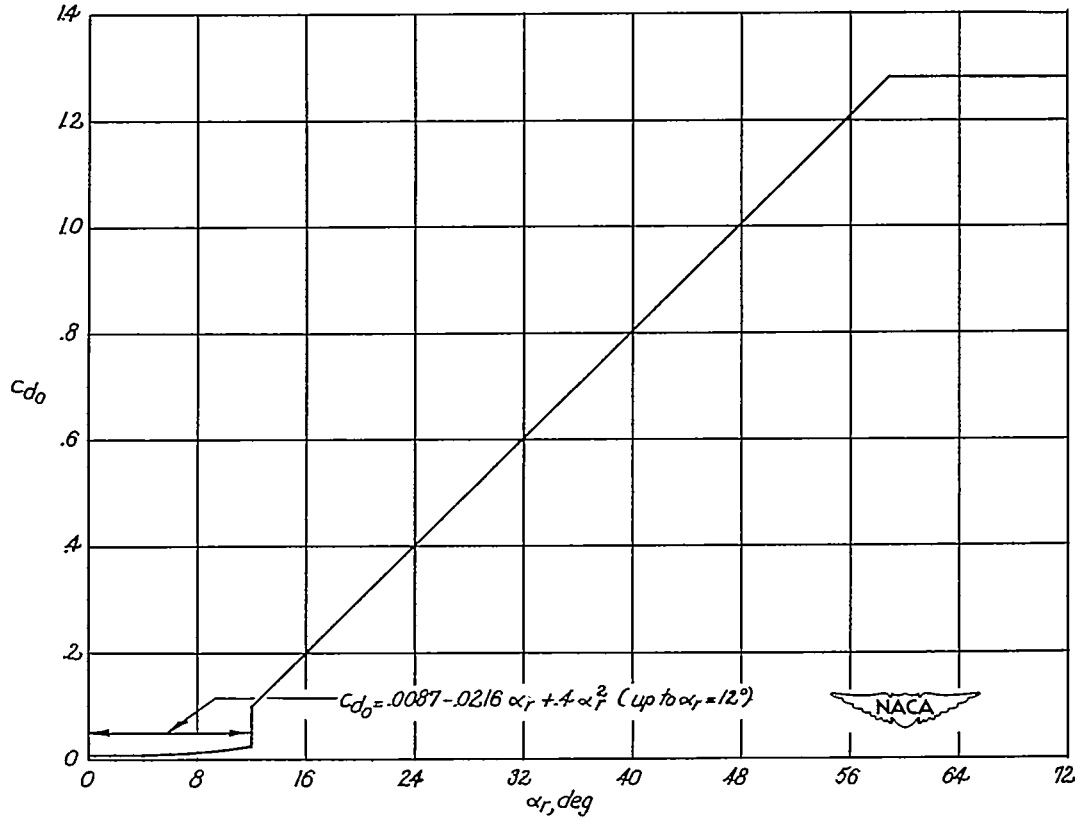

(b) c_{d_o} plotted against α_r.

Figure 2.- Lift and drag curves used in numerical evaluation of reversed-velocity region.

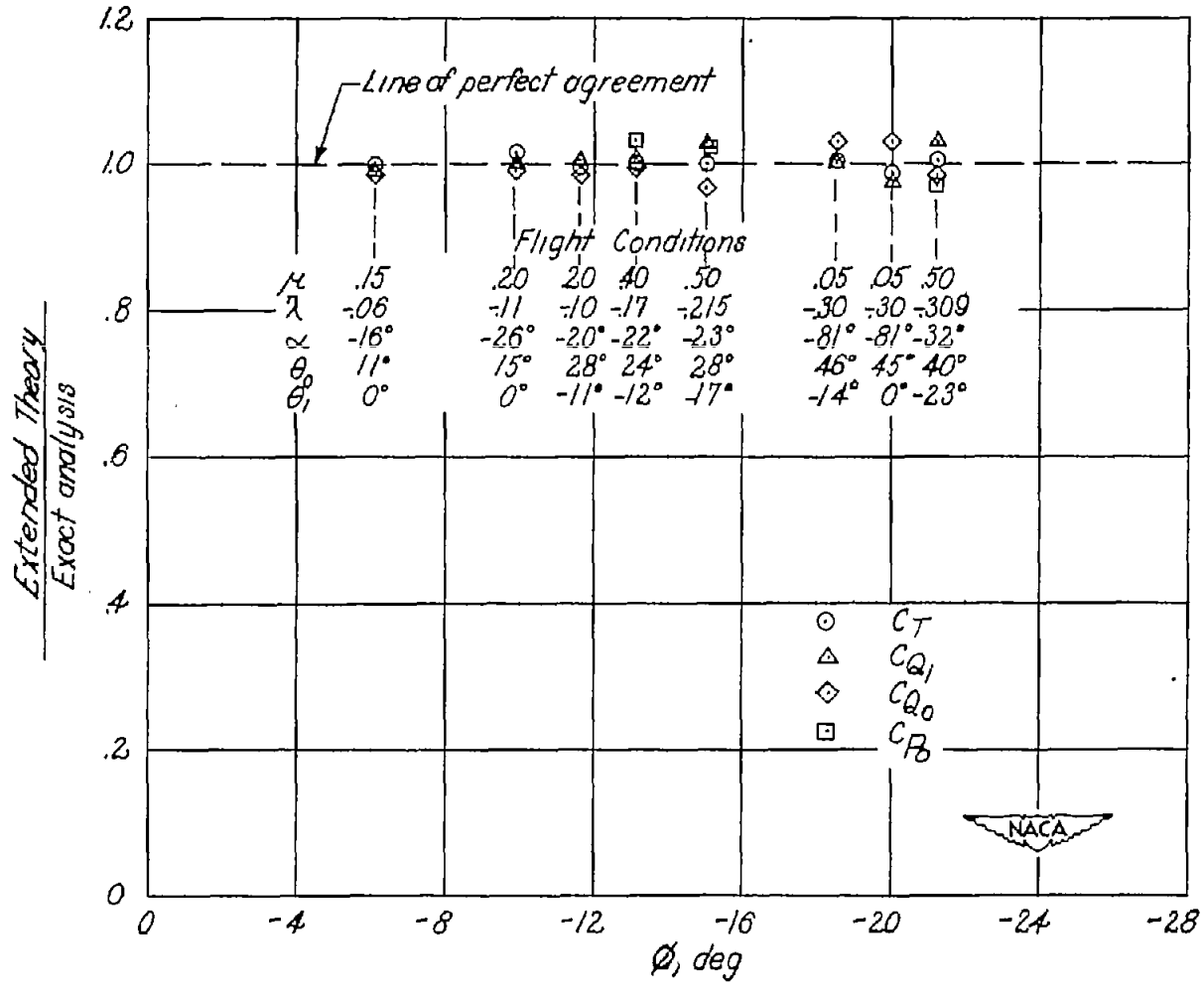

Figure 3.- Ratio of rotor characteristics as computed by extended rotor theory of present paper and an exact numerical integration analysis plotted against inflow angle at tip of advancing blade (i.e., at $x = 1.0$ and $\psi = 90^{\circ}$).

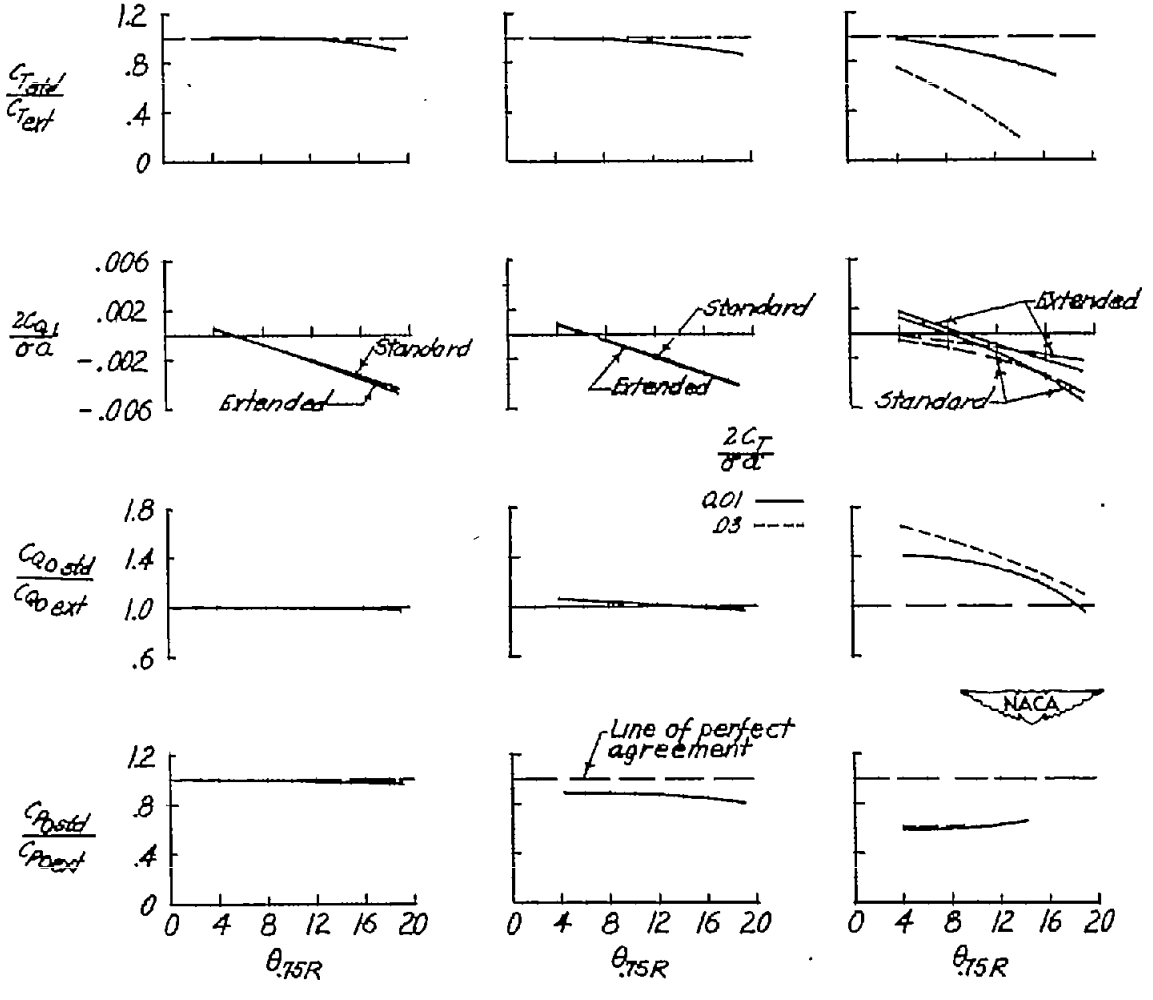

(a) $\mu = 0.10$. (b) $\mu = 0.30$. (c) $\mu = 0.50$.

Figure 4.- Comparison between standard and extended theory over a representative range of flight conditions; $\theta = -8^{\circ}$.

NACA-Langley - 4-28-53 - 1000